Supplemental Material

Blood-brain barrier resealing in neuromyelitis optica occurs independently of astrocyte regeneration

Anne Winkler[1], Claudia Wrzos[1], Michael Haberl[2], Marie-Theres Weil[3, 4], Ming Gao[5], Wiebke Möbius[3, 4], Francesca Odoardi[2], Dietmar R. Thal[6, 7], Mayland Chang[5], Ghislain Opdenakker[8], Jeffrey L. Bennett[9], Stefan Nessler[1], Christine Stadelmann[1]

[1] Institute of Neuropathology, University Medical Center Göttingen, Göttingen, Germany

[2] Institute for Multiple Sclerosis Research and Neuroimmunology, University Medical Center Göttingen, Göttingen, Germany

[3] Electron Microscopy Core Unit, Department of Neurogenetics, Max-Planck-Institute of Experimental Medicine, Göttingen, Germany

[4] Center Nanoscale Microscopy and Molecular Physiology of the Brain (CNMPB), Göttingen, Germany

[5] Department of Chemistry and Biochemistry, University of Notre Dame, Notre Dame, Indiana, USA

[6] Department of Imaging and Pathology, KU Leuven, and Department of Pathology, UZ Leuven, Leuven, Belgium

[7] Laboratory of Neuropathology, Institute of Pathology, Ulm University, Ulm, Germany

[8] Laboratory of Immunobiology, Department of Microbiology and Immunology, Rega Institute for Medical Research, KU Leuven, Leuven, Belgium

[9] Departments of Neurology and Ophthalmology, Program in Neuroscience, University of Colorado at Anschutz Medical Campus, Aurora, Colorado, USA

Address for correspondence:

Christine Stadelmann, MD
Institute of Neuropathology
Robert-Koch-Str. 40
37099 Göttingen, Germany
Tel.: +49-551-39-67570
e-mail: cstadelmann@med.uni-goettingen.de

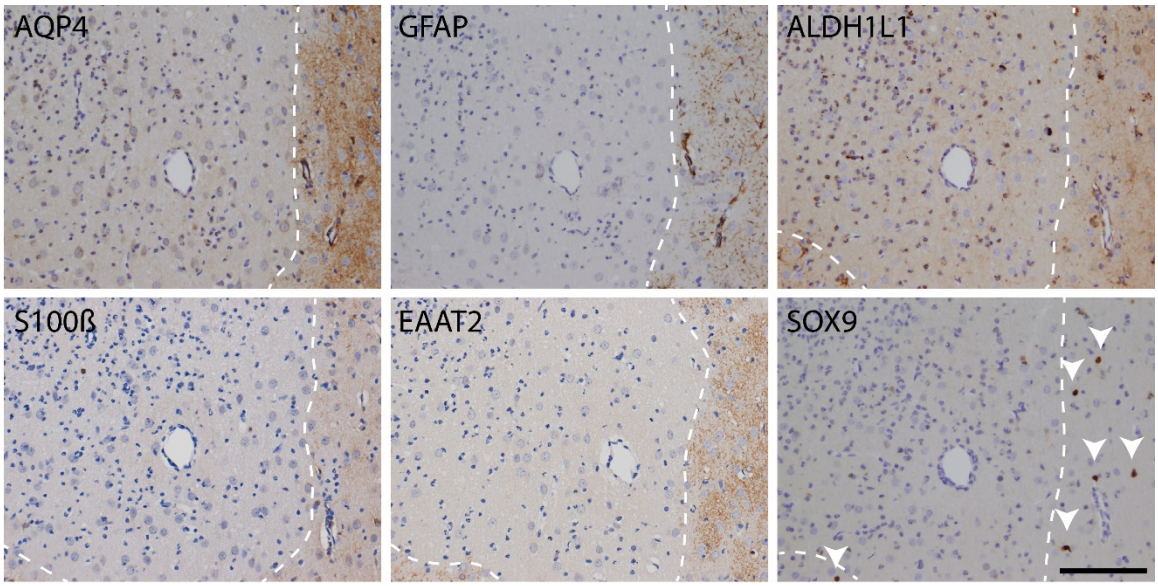

Supplemental Figure 1. Loss of astrocytes from experimental NMOSD lesions. Loss of astrocytes after focal cortical injection of AQP4-Ab and human complement was confirmed using immunohistochemistry for the astrocyte specific proteins AQP4, GFAP, ALDH1L1, S100ß, EAAT2 and the transcription factor SOX9. Loss of all markers was observed in experimental NMOSD lesions 24 h after lesion induction. Dotted line indicates lesion border. Arrowheads highlight SOX9 positive astrocyte nuclei next to the lesion. Scale bar 100 µm.

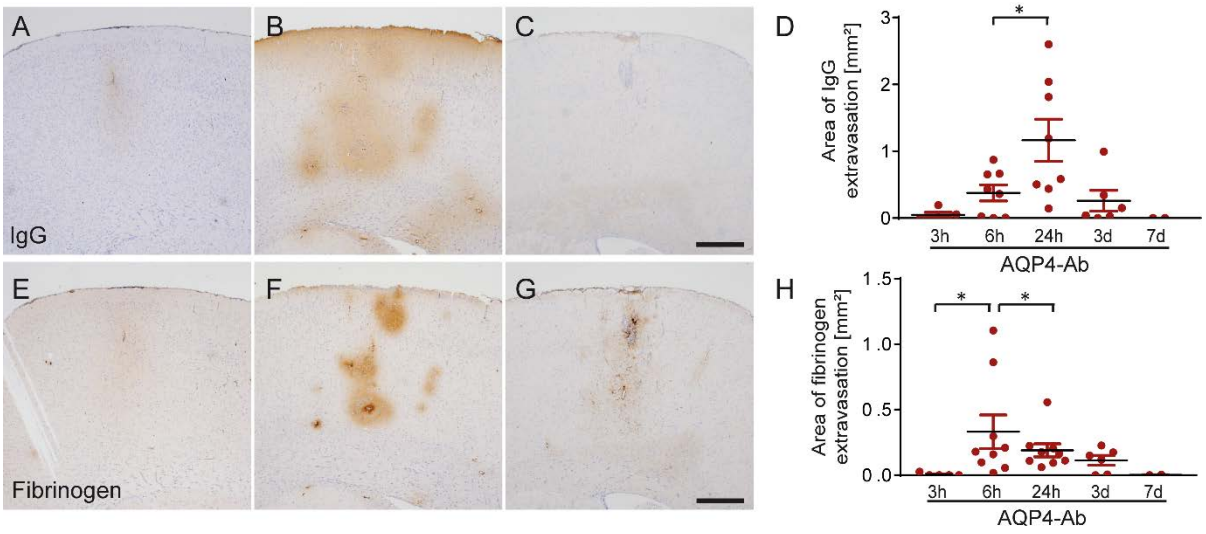

Supplemental Figure 2. Time course of endogenous tracer extravasation into the brain parenchyma. While IgG was observed only at very low amounts 3 h after lesion induction (A), extravasation was evident around blood vessels at 6 h (B), accumulated until 24 h and was cleared at 3 d (C; quantification: D; 3h n=5, 6h n=8, 24h n=8, 3d n=6, 7d n=2). Fibrinogen extravasation followed a similar time course with no leakage at 3 h (E), extravasation at 6 h (F) and deposit-like staining around blood vessels at 3 d (G; quantification: H; 3h n=5, 6h n=9, 24h n=9, 3d n=6, 7d n=2). D, H: Kruskal-Wallis test followed by Dunn's multiple comparison test *$p<0.05$. Graphs are shown as mean ± SEM. Scale bar A-C and E-G: 500 µm.

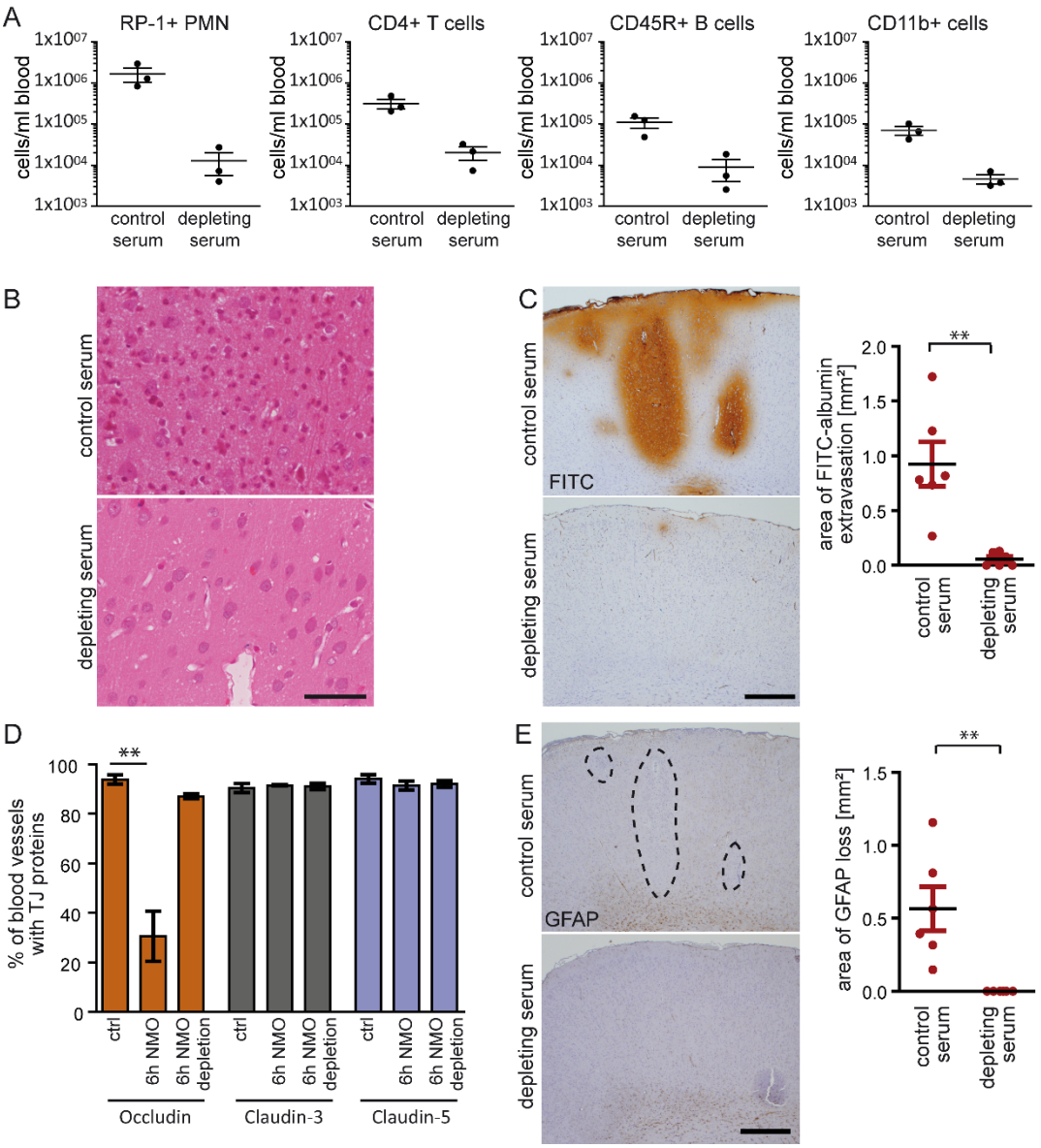

Supplemental Figure 3. Immune cell depletion prevents the formation of experimental NMOSD lesions 6 h after lesion induction. Treatment of rats with anti-PMN serum resulted in a strong reduction of PMNs, T cells, B cells and myeloid cells (A). In control serum treated rats, focal injection of AQP4-Ab together with human complement led to the infiltration of immune cells 6 h after lesion induction which was not seen in immune cell depleted rats reflecting the FACS blood results (HE stain, B). Moreover, immune cell depletion significantly decreased the permeability of the BBB to FITC-albumin 6 h after lesion induction (C). At the level of tight junctions, immune cell depletion rescued the loss of occludin. The localization of claudin-3 and claudin-5 at the tight junctions remained unaltered in immune cell depleted compared to control serum treated animals and healthy controls (ctrl n=3, 6 h AQP4-Ab anti-PMN and ctrl: n=4, D). Regarding astrocytes, control serum treated animals developed GFAP depleted lesions 6 h after focal injection of AQP4-Ab together with complement, which was prevented by immune cell depletion (E, dotted lines indicate area of GFAP loss). C-E: n=6, pooled data of 2 independent experiments. Mann-Whitney t-test *p<0.05, **p<0.01. Data are shown as mean ± SEM. Scale bar B: 50 µm, C, E: 500 µm.

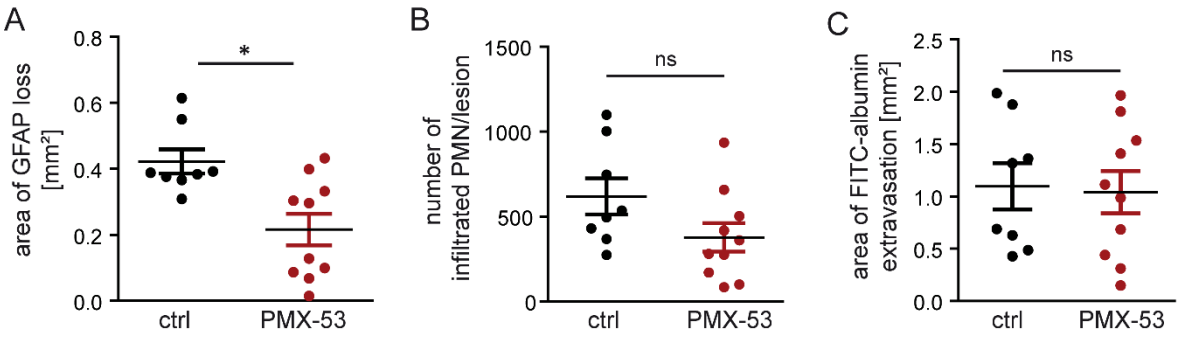

Supplemental Figure 4: Decreased astrocyte loss after systemic treatment with the C5aR antagonist PMX53 6 h after lesion induction. Rats were treated systemically with the C5aR antagonist PMX-53 and perfused 6 h after lesion induction with AQP4-Ab and human complement. Treatment with PMX-53 led to significantly less astrocyte loss compared to vehicle-treated animals (A), however, only a trend towards a reduced infiltration of PMNs was observed (p=0.083, B). PMX-53 treatment had no effect on BBB permeability as determined by FITC-albumin extravasation (C). Vehicle treated animals n=8, PMX-53 treated animals n=10, pooled data of 2 independent experiments. Mann-Whitney U test, *p<0.05, ns = not significant. Data are shown as mean ± SEM.

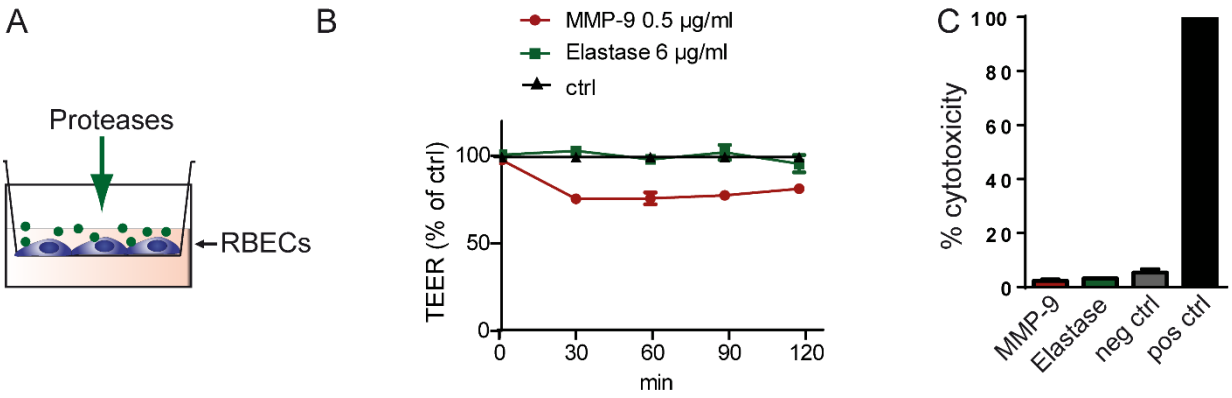

Supplemental Figure 5. MMP-9 reduces the transendothelial electrical resistance (TEER) of primary endothelial cells. Primary rat brain endothelial cells were seeded in the apical compartment of a transwell system to generate an in vitro BBB model. Proteases were added to the apical compartment and TEER was measured as a readout for BBB integrity (A). MMP-9, but not elastase, reduced TEER values in vitro compared to untreated controls (B, mean of 3 experiments performed in triplicates). The reduction in BBB integrity was not mediated by cytotoxicity as investigated using a LDH assay (C, 2 experiments performed in triplicates).

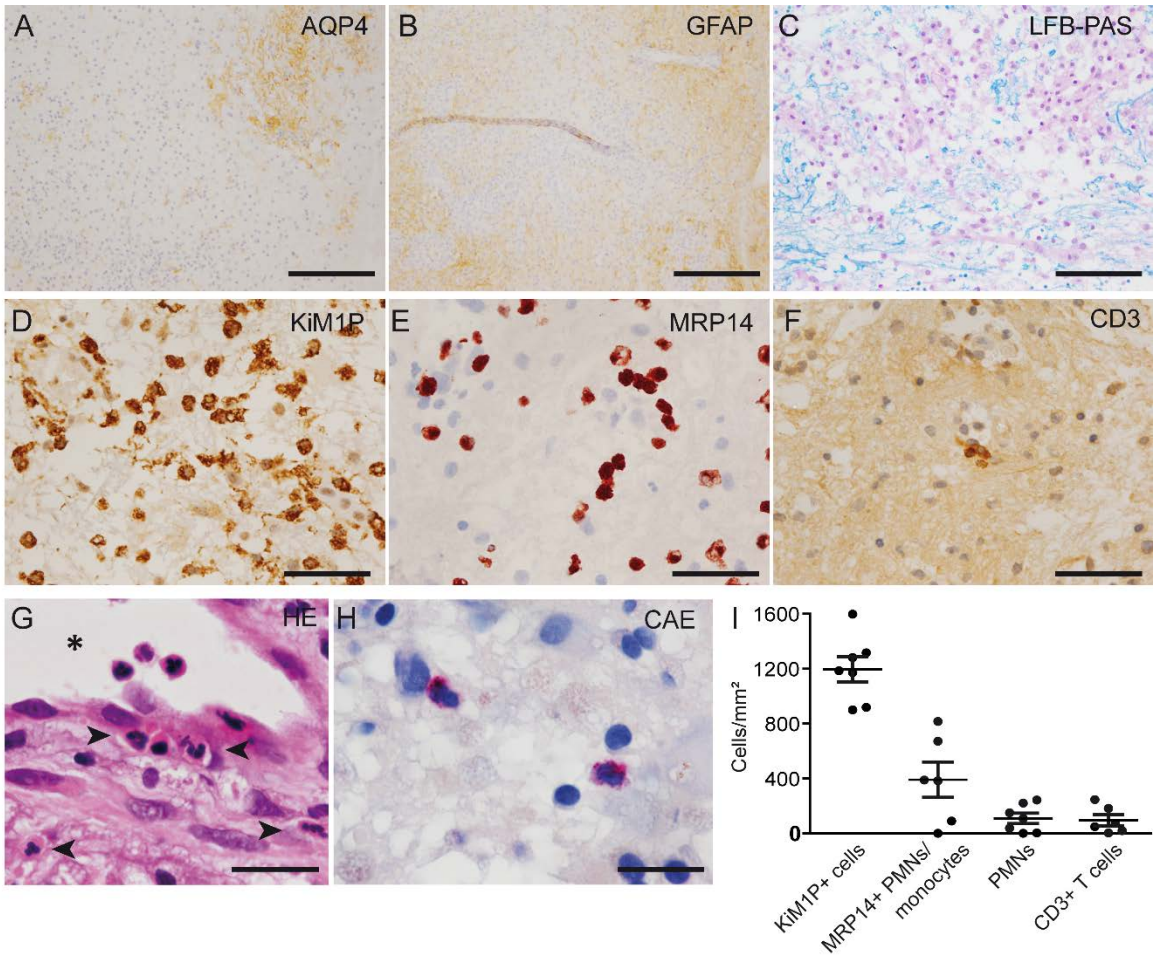

Supplemental Figure 6: Astrocyte loss and immune cell infiltration in human NMOSD lesions. Typical features of early human NMOSD lesions included astrocyte lysis and loss, whereby the area of AQP4 loss regularly exceeded that of GFAP loss (brown; A and B, respectively, patient 2), and incomplete demyelination (blue myelin in LFB-PAS stain, patient 3, C). The immune cell infiltrate consisted of abundant KiM1P-positive foamy macrophages/activated microglia (brown, patient 3, D), recently infiltrated monocytes and PMNs (MRP14, red-brown, patient 3, E), and scattered T cells (brown, patient 3, F). PMNs were identified by their multi-lobular nuclei (HE, arrowheads, patient 1, G) and in CAE histochemistry (pink, patient 2, H). Quantification in I (number of patients: KiM1P and PMN (HE) n=7, MRP14 and CD3 n=6). Scale bar A,B: 200 μm; C: 100 μm; D-F: 50 μm; G,H: 20 μm.

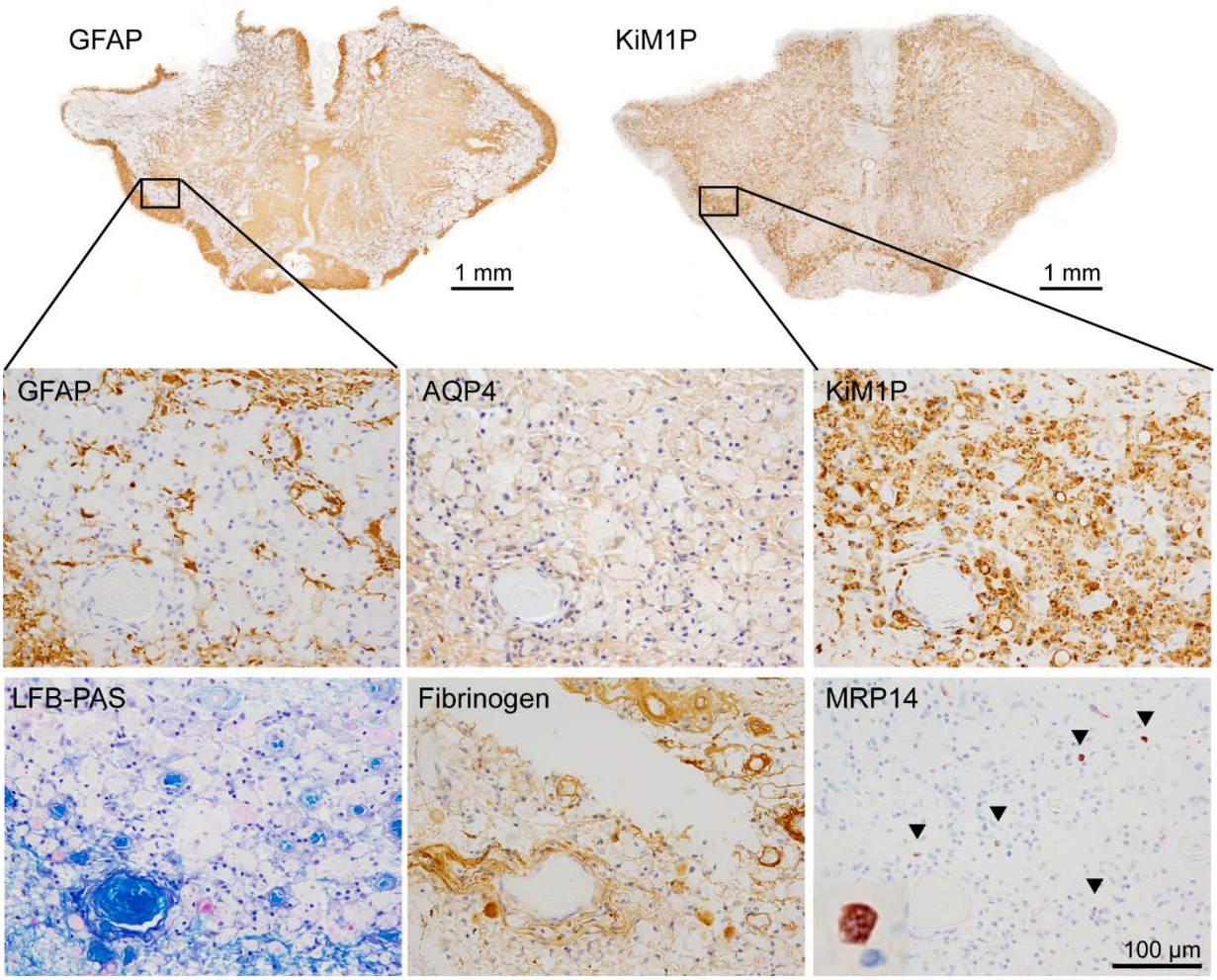

Supplemental Figure 7. Spinal lesion of NMOSD patient 7 – histological characterization. Tissue was obtained at autopsy and available for investigation of occludin and claudin-3 expression on frozen tissue and ultrastructural analysis of tight junctions. The NMOSD lesion investigated here extended over a major part of the spinal cord cross section and showed astrocyte loss with limited repopulation (GFAP and AQP4), a dense infiltration of foamy macrophages (KiM1P), and demyelination (LFB-PAS). Fibrinogen deposits were observed around vessels. This may indicate an open BBB or, alternatively, deposits that have not yet been cleared. Only few, if any, recently infiltrated MRP14 positive cells were detected.